SCIENCE CHINA
Technological Sciences

January 2010 Vol. 53 No.1: 200–205
doi: 10.1007/s11431-009-0311-1

Calculation of the extreme ultraviolet radiation of the earth's plasmasphere

HE Fei[1,4], ZHANG XiaoXin[2*], CHEN Bo[1] & FOK Mei-Ching[3]

[1] *Changchun Institution of Optics, Fine Mechanics and Physics, Chinese Academy of Sciences, Changchun 130033, China;*
[2] *National Center for Space Weather, China Meteorological Administration, Beijing 100081, China;*
[3] *NASA Goddard Space Flight Center, Greenbelt, MD 20771, USA;*
[4] *Graduated School of Chinese Academy of Sciences, Beijing 100039, China*

Received April 14, 2009; accepted June 24, 2009

The dynamic global core plasma model (DGCPM) is used in this paper to calculate the He^+ density distribution of the Earth's plasmasphere and to investigate the configurations and 30.4 nm radiation properties of the plasmasphere. Validation comparisons between the simulation results and IMAGE mission observations show: That the equatorial structure of the plasmapause is mainly located near 5.5 R_E and the typical scale of plasmasphere shrinking or expansion within 10 min is approximately 0.1 R_E; that the plasmaspheric shoulders are formed and rotate noon-ward from the dawn sector under the conditions of strong southward turning of the interplanetary magnetic field (IMF); that the plasmaspheric plumes will rotate dawn-ward from the night sector and become narrow for the southward turning of the IMF. The simulated images from the lunar orbit show that the plasmasphere locating within the geocentric distance of 5.5 R_E corresponds to field of view (FOV) of 10.7°×10.7° for the moon-based EUV imager, and that the 30.4 nm radiation intensity of the plasmasphere is 0.1–11.4 R. The plasmaspheric shoulders and plumes locating toward the moon-side are for the first time simulated with typical scale level of 0.1 R_E from the side view of the moon. These simulated results provide an important theoretical basis for the lunar-based EUV camera design.

earth's plasmasphere, dynamic global core plasma model, extreme ultraviolet radiation, lunar-based imaging

Citation: He F, Zhang X X, Chen B, et al. Calculation of the extreme ultraviolet radiation of the earth's plasmasphere. Sci China Tech Sci, 2010, 53: 200–205, doi: 10.1007/s11431-009-0311-1

1 Introduction

The earth's plasmasphere is a torus of cold, dense plasma region that occupies roughly the same region of the inner magnetosphere as the ring current and radiation belts between 2.0–7.0 R_E (R_E is the earth's radius). The typical electron density of plasmasphere is 10–10^4 cm^{-3}, with energy less than 1–2 eV and temperature ranging from 3000 to 5000 K [1, 2]. H^+ is the principle plasmaspheric ion (it's early called the photon-sphere). He^+ is the second abundant ion in the plasmasphere accounting for approximately 5%–10% of the plasmasphere plasma, and the ratio between He^+ and H+ changes with geomagnetic activities, ranging from 1% to 50% [3, 4]. The ions of plasmasphere are all trapped on magnetic field lines and form a field aligned distribution. The plasmasphere which strongly interacts with the ionosphere, ring current and radiation belt is the core region of inner magnetospheric interactions, and its evolutional process can affect the inner magnetospheric structure and near-earth space environment. Therefore, the research on plasmasphere has important scientific and practical value.

One distinct feature of the plasmasphere is to resonantly scatter the extreme ultraviolet (EUV) radiation of sunlight [5], and the scattering intensity is proportional to ion density

*Corresponding author (email: xxzhang@cma.gov.cn)

of the scattering point. Thus the best method to study the plasmasphere is to optically image the radiation and then inverse the images to get plasmaspheric ion densities. The plasmaspheric EUV radiation contains two main lines: 30.4 nm by He^+ and 83.4 nm by O^+. The former is a line spectra with scattering rate between 1.8×10^{-5}–3.4×10^{-5} photons $\cdot$ ion$^{-1}\cdot$ s^{-1} [6], and the later is triplet spectra containing 9 lines with scattering rate between 1.0×10^{-7}–9.4×10^{-7} photons $\cdot$ ion$^{-1}\cdot$ s^{-1} [7]. Other ions also emit EUV radiations, but they are inapposite to detect because of their extremely low abundance. The advantage of selecting 30.4 nm emission also lies in that He^+ is the second abundant ion in the plasmasphere (~10%, but O^+ is less than 1%), and its distributions and dynamic properties can represent the overall plasmasphere. The 30.4 nm emission is a single line which is the strongest radiation of plasmasphere, and the magnetosphere is optically thin to the line [8]. The background emissions can be neglected, so the detection and the calculation are simple and accurate. In addition, the response time of optical imaging is short in that one image can be shot in just several minutes. The image is intuitive, which is suitable for observations and researches on the response of plasmasphere to geomagnetic activities during storms and substorms as well as for space weather monitoring and forecasting.

In this paper, we will briefly describe the dynamic global core plasma model (DGCPM) which can be used to calculate the particle distribution of the plasmasphere in Section 2 and then compare the modeled plasmasphere with observation results in Section 3. More emphases are focused on analyzing the storm time plasmasphere evolutions and discussing the current problems of the plasmaspheric researches. We also investigate the method of imaging the plasmasphere from the side views (lunar orbit), analyze its feasibility, and optimize the parameters of EUV camera in this section.

2 Simulating the 30.4 nm radiation intensity

The plasmaspheric He^+ resonantly scatters the 30.4 nm radiation of the sun, and the column integrated intensity I along a given line of sight (LOS) direction L with the element ds is

$$I = 1/4\pi\int_L \mathrm{e}^{-\tau} p(\theta) g n(r)\mathrm{d}s\times10^{-6}, \tag{1}$$

where I is the column integrated intensity (photons cm^{-2} s^{-1}), $p(\theta)$=1+1/4(2/3–sin^2 θ) is the phase function [9], θ is the angle between the incident direction (sun-earth) and scattered direction in the direction of the camera, g is the resonant scattering rate of He^+ (photons s^{-2} ion^{-1}, related with solar 30.4 nm radiation flux and He^+ quantum mechanics properties, can be seen as a constant during an image period), $n(\boldsymbol{r})$ is the density in cm^{-3} at position $\boldsymbol{r}$, and τ is the optical depth of 30.4 nm line. Since the magnetosphere is optically thin above 1000 km (~1.2 R_E) τ can be set to zero.

The core of modeling He^+ 30.4 nm radiation intensity is to model the He^+ density distribution. The DGCPM was used in this study [10]. The dynamical evolution process of the plasmasphere was achieved through flux tube convection method. Assume that the density along a magnetic flux tube is constant and its density is determined by the flux in or out of the tube at the ionosphere

$$\frac{D_\perp N}{Dt} = \frac{F_n}{B_{ni}} + \frac{F_s}{B_{si}}, \tag{2}$$

where $D_\perp/Dt$ is the convection derivation in the moving frame of the flux tube, N is the total ion content per unit flux, F_s and F_n are the flux in or out the flux tube at the northern and southern ionospheres, B_{si} and B_{ni} are the magnetic fields in the northern and southern ionospheres at the foot point of the flux tube [11, 12]. This first order hyperbolic partial differential equation can be solved to get the He^+ density distribution of the plasmasphere.

In the simulation, the magnetic field model and electric field model should be considered in the plasmaspheric region. Since there was no global magnetic and electric observation data available for the inner magnetosphere, the empirical models were adopted in our simulations. In our calculations we used the international geomagnetic reference field (IGRF) model and Tsyganenko geomagnetic field model, which includes the contributions from the inner geomagnetic field and external magnetospheric sources: the ring current, magnetotail current system, magnetopause currents, and the large-scale system of field-aligned currents [13]. The electric field model used in our calculations was the Weimer model, which reflects the impacts of solar wind and interplanetary magnetic field on middle and high latitude ionospheric electric fields [14], and is more appropriate to simulate observation data. When simulating the plasmaspheric evolution, the magnetic flux tubes were initialed with saturated plasmasphere [15], and the plasmasphere was convected for 5 days to reach an equilibrium state under weak solar wind conditions. Then the plasmasphere was imposed and driven by a strong convection so as to investigate its structure and evolution during storm times.

3 Simulation and observation results

The EUV camera on board the IMAGE spacecraft, a NASA's mission operated during 2000–2005, imaged for the first time the overall plasmasphere at the apogee region of a polar orbit using optical method and derived two dimensional global images of the plasmasphere projected on the magnetic equatorial plane. In this section, we will analyze two storm cases observed by IMAGE/EUV imager and compare them with the results from the DGCPM.

3.1 Storm on 24 May 2000

During the strong magnetic storm on 24 May 2000 as shown in Figure 1, the components of the IMF B_Y and B_Z reached −20.0 nT, the solar wind speed V_{SW} exceeded 700 km/s, and the *Dst* index reached −150.0 nT with the maximum *Kp* index of 8.0. During the period (indicated by the gray region), the IMF had a strong southward turning, the solar wind velocity increased continuously, and *Dst* index decreased continuously and reached the maximum absolute value, corresponding to the turning stage of main phase and recovery phase of the storm. During this stage, the plasmasphere was eroded by this strong magnetospheric convection and shrank inward, the sunside plasmapause shrank to approximately 2.0 R_E, and the nightside plasmapause shrank to approximately 3.0 R_E. The width of the plume became narrow and the shoulder turned noon-ward as shown in Figure 2(a). Figure 2(b) represents the simulation results of the DGCPM with the input parameters of the gray region in Figure 1. In the simulation, the rotating speed of the shoulder and the nightside plasmapause were basically consistent with the observations. The dayside plasma-pause was slightly larger than the observations. This slight dissimilarity might be caused by the fact that the magnetic field pattern in the simulation was different from the actual pattern and the convection electric field was stronger than the actual electric field, causing the sunward convection to become stronger.

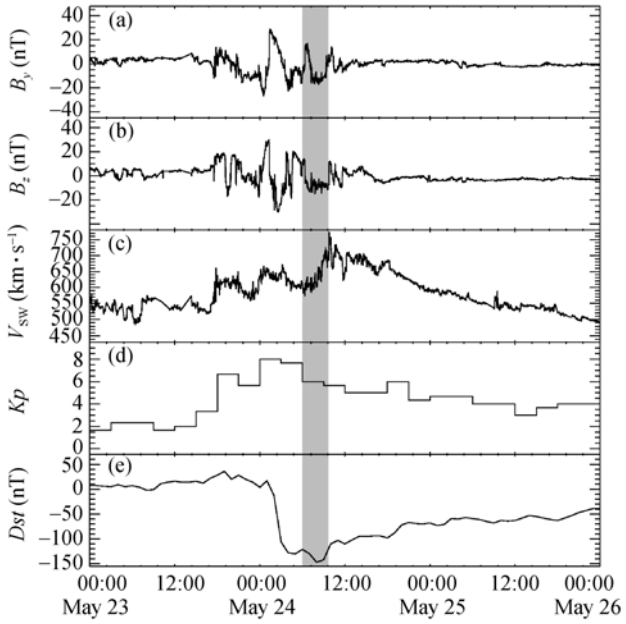

Figure 1 Geomagnetic index, solar wind and interplanetary magnetic field (IMF) parameters of 24 May 2000 storm. The gray region is the time sector for simulation. (a) *Y* component of IMF; (b) *Z* component of IMF; (c) solar wind speed; (d) *Dst* index; (e) *Kp* index.

3.2 Storm on 26 June 2000

The magnetic storm that happened on 26 June 2000 was weaker than that on 24 May as shown in Figure 3, both the components of the interplanetary magnetic field B_Y and B_Z were less than −20.0 nT, the solar wind velocity V_{SW} was less than 550 km/s, and the *Dst* index was less than −100.0 nT with the maximum *Kp* index of 6.0. During the period represented by the gray region, the interplanetary magnetic field also had a south-ward turning, the solar wind velocity increased continuously, and *Dst* index decreased continuously and reached the maximum absolute value. During this stage, the plasmasphere was eroded by relatively strong magnetospheric convection and shrank continuously, and the plasma-

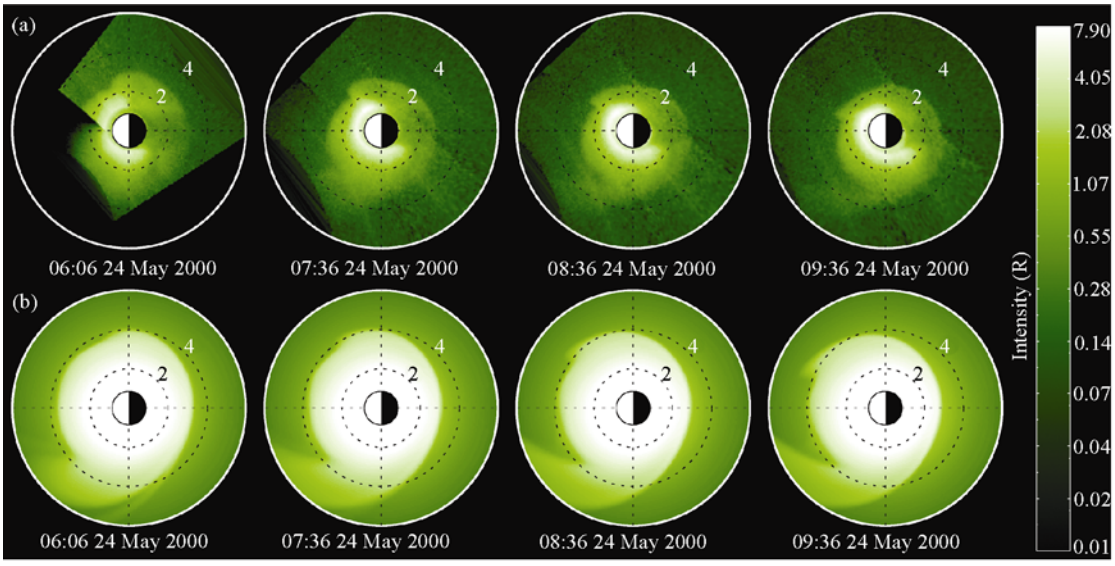

Figure 2 Observations and simulation results for 24 May 2000 storm, the earth radii represented by the dashed circles were shown in the images. (a) IMAGE observation; (b) DGCPM simulation.

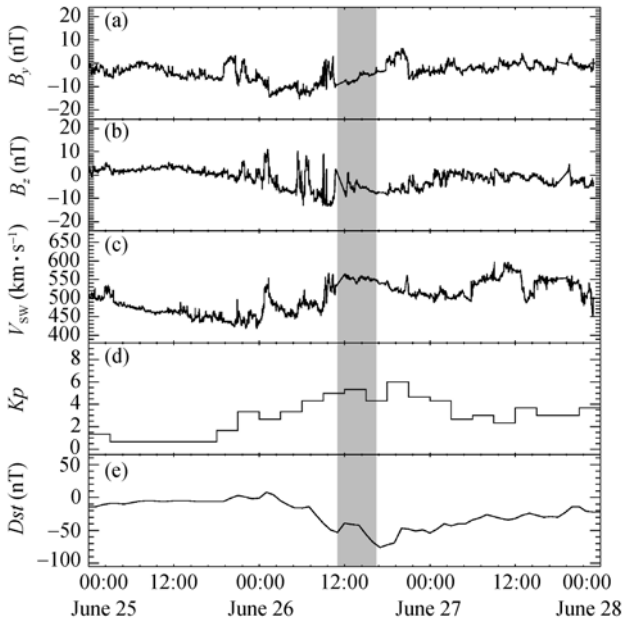

Figure 3 Geomagnetic index, solar wind and interplanetary magnetic field (IMF) parameters of 26 June 2000 storm. The gray region is the time sector for simulation. (a) *Y* component of IMF; (b) *Z* component of IMF; (c) solar wind speed; (d) *Dst* index; (e) *Kp* index.

pause shrank to approximately 3.0 R_E. The plume narrowed as time went on and rotated dusk-ward (see Figure 4(a)). No shoulder was formed in this case. Figure 4(b) represents the simulation results of DGCPM with the parameters of the gray sector in Figure 3. The simulation results were approximately consistent with the observations. Both the dayside and nightside plasmapauses were consistent with the observation, keeping at 3.0 R_E. The only difference was that the rotating speed in the simulation was less than the observation result.

3.3 Imaging the plasmasphere from the side views

We have simulated the plasmaspheric images from the lunar orbit using the DGCPM. We assumed an EUV camera on the moon which viewed towards the center of the earth. The field of view was 15° (corresponding to the spatial size of 15.0 R_E). The spatial resolution of the image was 0.1 R_E on the projection plane (the plane crosses the center of the earth and perpendicular to the normal of the camera). Nine points in the lunar orbit from lunar dawn to lunar dusk were selected as shown in Figure 5 to investigate the intensity distributions from different positions. In order to investigate the shoulder and plume evolution from the side views, the simulation time of UT09:36 24 May 2000 was selected, and the corresponding solar wind conditions are shown in Figure 1.

The intensity of the He^+ 30.4 nm emission from the plasmasphere (within the plasmapause) as shown in Figure 6 was 0.1–11.4 R. This result was consistent with early measurements of 0.1–10 Rayleigh done by sounding rockets [16], consistent with simulated EUV images of 0.1–15 R of the plasmasphere [17], and with the measurements of 0.1–7 Rayleigh done by Planet-B mission [18]. According to the measurements of GEOTAIL satellite [19] and our simulations, the density of the He^+ beyond 5.5 R_E was quasi-stable, with a density of 0.2–2.0 cm^{-3} and a corresponding column integrated intensity of 0.026–0.13 Rayleigh. The intensity in the plasmasphere trough region outside the plasmapause was approximately 0.02–0.1 Rayleigh, which was consistent with the observations.

The images of plasmaspheric shoulders and plumes were

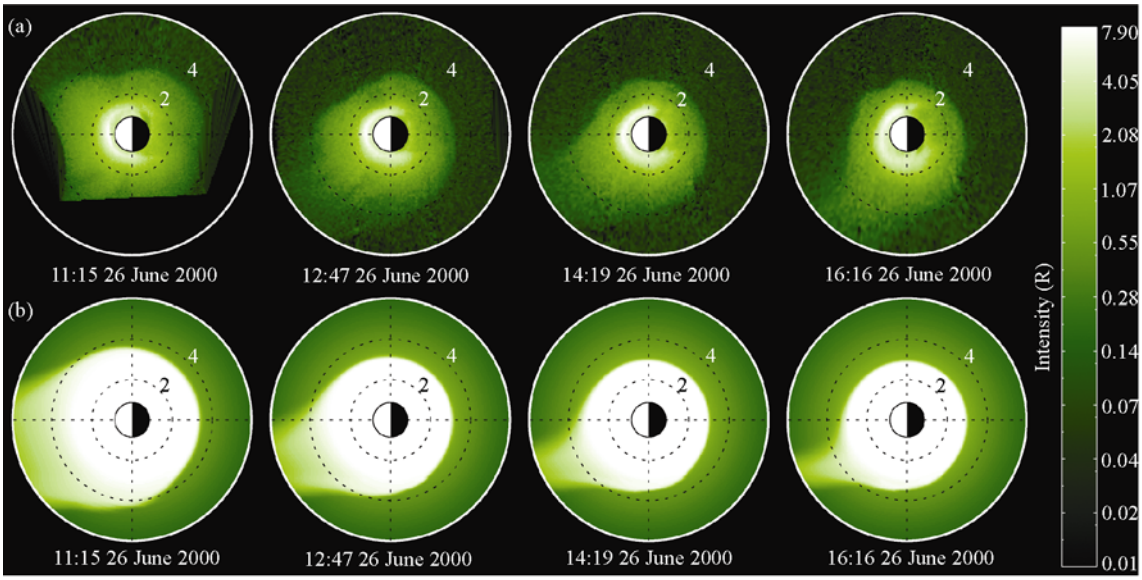

Figure 4 Observations and simulation results for 26 June 2000 storm, the earth radii represented by the dashed circles were shown in the images. (a) IMAGE observation; (b) DGCPM simulation.

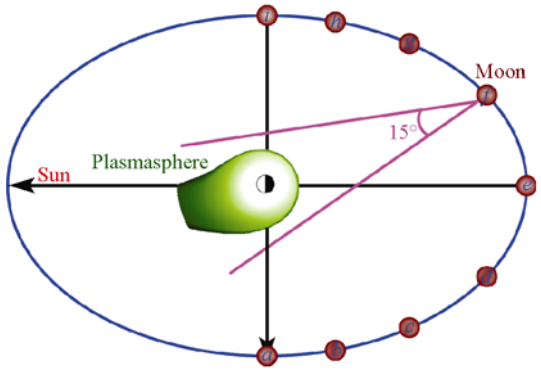

Figure 5 Cartoon for lunar positions of the simulation. The SM coordinates for positions *a*–*i* are (0, 60.0, 0), (–22.4, 54.3, 2.0), (–40.7, 40.8, 3.7), (–52.5, 21.9, 4.7), (–56.6, 0, 5.1), (–52.5, –21.9, 4.7), (–40.7, 40.8, 3.7), (–22.4, –54.3, 2.0), (0, –60.0, 0), respectively in unit of R_E.

modeled from the side view for the first time. At different positions, because the LOS directions and the projection directions were different, the shapes and positions of the plumes in the images were different (see the white rectangle regions in Figure 6). The closer the moon to its dawn or dusk, the less distinct the plumes in the images, due to the shielding and overlapping effect of the LOS integration. The plasmaspheric shoulders were distinct only in images of Figures 6(d)–(g) (see the dashed rectangle regions). The shoulders were not evident at other positions because of the line overlapping effect and because the spatial size of the shoulder was approximately 0.2 R_E. In addition, the plasmaspheric shoulders observed from the moon were not as apparent as that of polar orbit because of the shielding of the main body of the plasmasphere.

As is shown in Figure 6, at different positions of the lunar

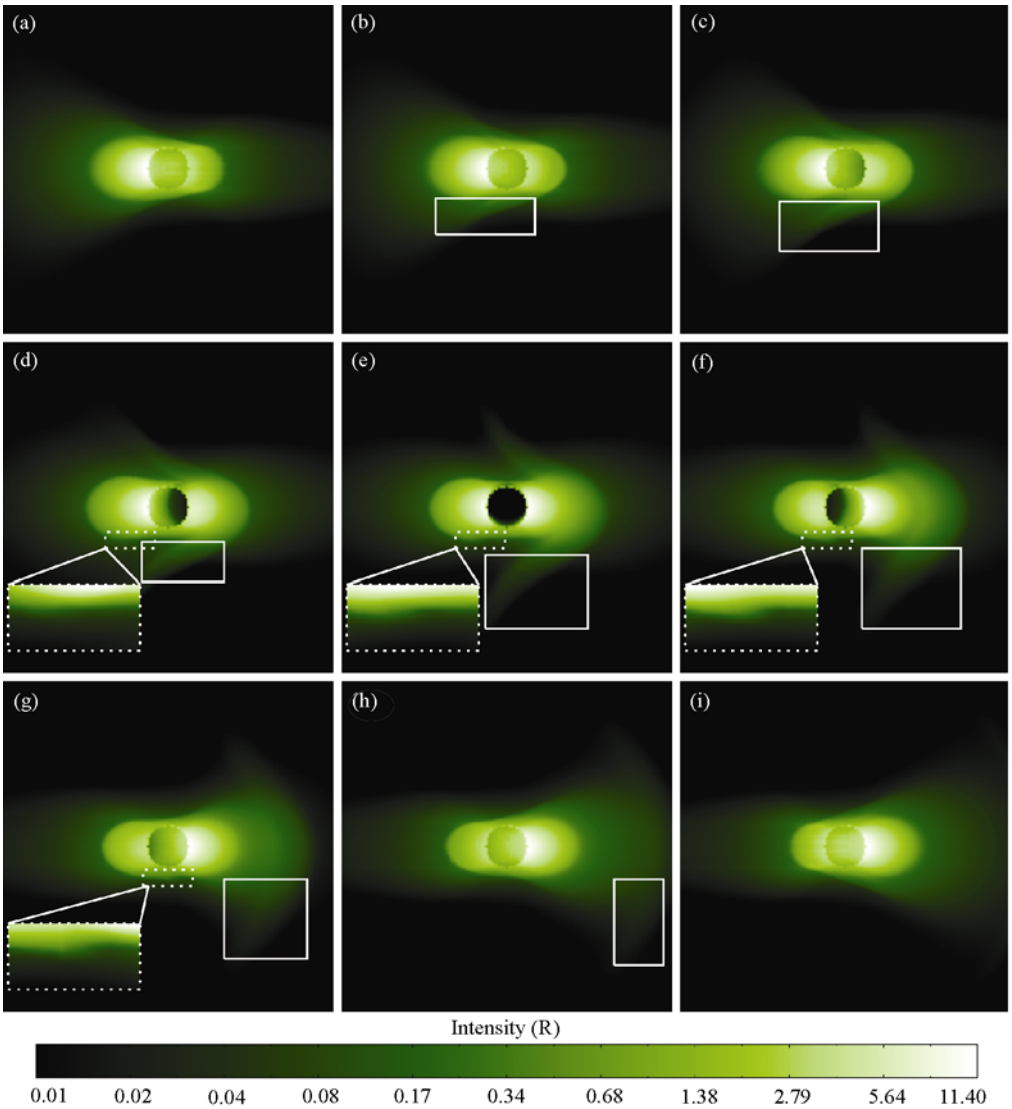

Figure 6 EUV radiation intensity distributions of the earth's plasmasphere form different positions of the lunar orbit. (a)—(i) Represent the intensities of the positions shown in Figure 5 respectively, the dashed rectangle regions represent the regions of shoulders, and the white rectangle regions represent the regions of plumes. The dashed rectangle regions at the lower left corners of (d)—(g) represent the amplified shoulder regions.

orbit, the main body of the plasmasphere (the plasmasphere, plume, shoulder) was within 5.5 R_E, which was consistent with the observations of IMAGE/EUV. Thus, a field of view of 10.7°×10.7° and spatial resolution of 0.1 R_E (average moon-earth distance of 60.0 R_E) can image the overall plasmasphere effectively and meets the requirements of scientific research on the plasmasphere.

4 Conclusions

We used the DGCPM to simulate the dynamic structure and radiation properties of the plasmasphere, compared them with the observations of IMAGE mission and calculated the plasmaspheric EUV radiation intensities from different observing positions on the moon. The main results are as follows.

(1) The plasmasphere was within 5.5 R_E on the magnetic equatorial plane and within 4.0 R_E on the meridian plane. The typical scale size of the plasmapause, shoulder and plume were 0.1 R_E. A field of view of 10.7°×10.7° and spatial resolution of 0.1 R_E (average moon-earth distance of 60.0 R_E) are needed for the lunar-based EUV imager.

(2) The average velocity of erosion or refilling of the plasmapause during storm time observed by IMAGE mission was approximately 0.7 R_E/h [20, 21], corresponding to the equivalent spatial resolution, 0.1 R_E in 10 minutes. Thus time resolution of 10 min or better is needed for the lunar-based EUV imaging.

(3) When imaging from the side view, the 30.4 nm emission intensity was 0.1–11.4 Rayleigh within the plasmapause and 0.02–0.1 Rayleigh outside it. The observation scope of EUV camera should meet this requirement.

This investigation provides a theoretical basis for the design of the lunar-based EUV camera. This EUV camera may image the overall plasmasphere continuously and effectively, which is favorable to carry out researches on physical properties and space weather forecasting of the earth's plasmasphere.

This work was supported by the National Natural Science Foundation of China (Grants No. 40774098, 40774079 and 40890160), the National Hi-Tech Research and Development Program of China ("863" Project) (Grant No. 2007AA12Z314), and the Chinese Academy of Sciences Innovation Program. The authors would like to thank Dr. Weimer D R for providing the Weimer electric field model and Dr. Gallagher D L for valuable discussions on this paper. The authors would like to thank NASA-CCMC (http://ccmc.gsfc.nasa.gov/) for providing the code of IGRF and Tsyganenko model and Dr. Forrester T of IMAGE/EUV team for the EUV data and relevant processing software available at http://euv.lpl.arizona.edu/euv/. The authors also thank the ACE Science Center for the MAG and SWEPAM data available at http://www.srl.caltech.edu/ACE/ASC/, and the Kyoto World Data Center for the geomagnetic index available at http://swdcwww.kugi.kyoto-u.ac.jp/index. html.

1 Horwitz J L, Brace L H, Comfort R H, et al. Dual-spacecraft measurements of plasmasphere-ionosphere coupling. J Geophys Res, 1986, 91(A10): 11203–11216
2 Chiu Y T, Luhmann J G, Ching B K, et al. An equilibrium model of plasmasphere composition and density. J Geophys Res, 1979, 84(A3): 909–916
3 Farrugia C J, Geiss J, Young D T, et al. GEOS-1 observations of low-energy ions in the earth's plasmasphere: a study on composition, and temperature and density structure under quiet geomagnetic conditions. Adv Space Res, 1988, 8(1): 25–33
4 Farrugia C J, Geiss J, Young D T, et al. The composition, and temperature and density structure of cold ions in the quiet terrestrial plasmasphere: GEOS-1 results. J Geophys Res, 1989, 94(A9): 11865–11891
5 Meier R R. Ultraviolet spectroscopy and remote sensing of the upper atmosphere. Space Sci Rev, 1991, 58: 1–185
6 Garrido D E, Smith R W, Swift D W, et al. Imaging the plasmasphere and trough region in the extreme ultraviolet region. Opt Eng, 1994, 33(2): 371-382
7 Garrido D E, Smith R W, Swift D W, et al. Imaging the Earth's magnetosphere: Effects of plasma flow and temperature. Planet Space Sci, 39(11): 1559–1571
8 Brandt J C. Interplanetary gas, VI, On diffuse extreme ultraviolet helium radiation in the night and day sky. Astrophys J, 1961, 134: 975–980
9 Brandt J C, Chamberlain J W. Interplanetary gas, I, Hydrogen radiation in the night sky. Astrophys J, 1959, 130: 670–682
10 Ober D M, Horwitz J L, Gallagher D L. Formation of density troughs embedded in the outer plasmasphere by subauroral ion drift events. J Geophys Res, 1997, 102(A7): 595–602
11 Chen A J, Wolf R A. Effects on the plasmasphere of a time-varying convection electric field. Planet Space Sci, 1972, 20(4): 483–509
12 Rasmussen C E, Guitar S M, Thomas S G. A two dimensional model of the plasmasphere: Refilling time constant. Planet Space Sci, 1993, 41(1): 35–43
13 Tsyganenko N A, Sitnov M I. Modeling the dynamics of the inner magnetosphere during strong geomagnetic storms. J Geophys Res, 2005, 110(A03208), doi: 10.1029/2004JA010798
14 Weimer D R. Improved ionospheric electrodynamic models and application to calculating Joule heating rates. J Geophys Res, 2005, 110(A05306), doi: 10. 1029/2004JA010884
15 Carpenter D L, Anderson R R. An ISEE-Whistler model of equatorial electron density in the magnetosphere. J Geophys Res, 1992, 97(A2): 1097–1108
16 Ogawa T, Tohmatsu T. Sounding rocket observation of helium 304- and 584-Å glow. J Geophys Res, 1971, 76(25): 6136–6145
17 Roelof E C, Mauk B H, Meier R R. Instrument requirements for imaging the magnetosphere in extreme ultraviolet and energetic neutral atoms derived from computer-simulated images. Proc SPIE, 1992, 1744(1): 19–30
18 Nakamura M, Yoshikawa I, Yamazaki A, et al. Terrestrial plasmaspheric imaging by an extreme ultraviolet scanner on Planet-B. Geophys Res Lett, 2000, 27(2): 141–144
19 Matsui H, Mukai T, Ohtani S, et al. Cold dense plasma in the outer magnetosphere. J Geophys Res, 1999, 104(A11): 25077–25095
20 Murakami G, Hirai M, Yoshikawa I. The plasmapause response to the southward turning of the IMF derived from sequential EUV images. J Geophys Res, 2007, 112(A06217), doi: 10. 1029/2006JA012174
21 Goldstein J, Sandel B R, Forrester W T, et al. IMF-driven plasmasphere erosion of 10 July 2000. Geophys Res Lett, 2003, 30(3): 1146, doi: 10.1029/2002GL016478